Dyes and Pigments 202 (2022) 110244

Contents lists available at ScienceDirect

Dyes and Pigments

journal homepage: www.elsevier.com/locate/dyepig

# Pyridyl anchored indolium dyes for the p-type dye sensitized solar cell

Anil Reddy Marri [a], Heather Flint [b], Elizabeth A. Gibson [b,**], John Fielden [a,*]

[a] School of Chemistry, University of East Anglia, Norwich Research Park, Norwich, NR4 7TJ, United Kingdom
[b] School of Chemistry, Newcastle University, Newcastle-upon-Tyne, NE1 7RU, UK

## ABSTRACT

Three new thiophenyl bridged triarylamine-donor based dyes with pyridyl anchoring groups and indolium acceptors have been synthesized and studied as sensitizers for the p-type dye-sensitized solar cell (p-DSSC). Compared to known dicyano and pyridinium dyes with the same triarylamine cores, these new sensitizers have broadened and red-shifted UV–vis absorption spectra, with high extinction coefficients and absorption extending beyond 700 nm. TD-DFT calculations on the indolium family indicate that these dyes combine strong donor acceptor communication, with a high degree of charge separation in the excited state – an ideal combination for sensitizer dyes. The phenylpyridyl anchored *bis*-indolium gives the highest power conversion efficiency (0.097%) through a short circuit photocurrent ($J_{SC}$) of 3.04 mA cm$^{-2}$, open circuit voltage ($V_{OC}$) of 97 mV and fill factor of 36%. This exceeds the performance of the **P1** reference dye in this study, and represents the best performance so far for a cationic, pyridine anchored p-DSSC dye.

## 1. Introduction

Since the first report in 1991 by Grätzel and O'Regan, dye-sensitized solar cells (DSSCs) have been one of the most prominent alternatives to conventional Si-based solar cells [1]. These devices, with best reported efficiencies of *ca.* 14% [2], lag behind the peak performance of Si but are finding applications in indoor and building-integrated photovoltaics as they function much better than Si in low and diffuse light conditions. Compared to Si, whose band gap corresponds to an 1100 nm photon, DSSCs struggle to harvest low energy photons because the dye HOMO – LUMO gap must exceed the energy difference between the redox mediator and conduction band edge. In 1999 Lindquist et al. proposed that light harvesting performance could be improved by replacing the DSSC's platinized cathode with a dye-sensitized photocathode that would collect lower energy photons, increasing spectral coverage and photovoltage ($V_{OC}$) in the resulting tandem cell [3]. This leads to a theoretical maximum efficiency of 43%, vs 33% for a single junction device.

In p-DSSCs, a sensitizer dye injects holes into the valence band of a p-type semiconductor (p-SC, typically NiO), and the reduced dye is then oxidised by the redox mediator. So far, the power conversion efficiencies (PCEs) of p-DSSCs have remained low - the highest reported is only 2.5% [4], achieved using a redox mediator with a relatively negative redox potential to maximise $V_{OC}$. But such mediators inevitably reduce the photovoltage produced by the more efficient n-type side of any tandem cell. With more $TiO_2$ compatible mediators, the record PCE remains below 1.5% [5], and the record PCE of a pn-tandem cell is only 4.1% [6]. A number of factors, including rapid recombination of photogenerated holes from NiO to the electrolyte, slow hole transfer through NiO, and the small energy difference between the NiO VB and redox mediator contribute to this low performance [4–7].

Consequently, substantial efforts have been invested both in the design and synthesis of new dyes that can mitigate these problems, and the discovery of new p-SCs with better fundamental properties [8]. The largest and most successful class of sensitizers has been neutral organic chromophores based on triphenylamine (TPA) donor groups that anchor to NiO via carboxylates, with a wide range of bridges and acceptors designed to maximise light absorption and reduce recombination by moving electrons away from the NiO surface [4–9]. However, it has been suggested that pyridyl binders can be competitive and give high $V_{OC,}$ [11] and their softer N-donor may potentially be more suitable for binding alternative p-SCs. Moreover, we have recently found that, compared to commonly used dicyano acceptor groups, quaternized N-heterocycles (indolium, and pyridinium) both give stronger and broader light absorption that extends further into the red [10,12]. Devices based on dyes using these acceptors have shown performances that generally exceed those of comparable dicyano systems on a per dye (if not absolute) basis, and the best indoliums have produced record $J_{SC}$ [13]. An additional attraction of these acceptors is their synthetic accessibility, and the scope for tailoring properties by adjusting the quaternizing group.

Herein, we present the synthesis, photophysical and electrochemical

---

[*] Corresponding author.
[**] Corresponding author.

*E-mail addresses:* Elizabeth.Gibson@newcastle.ac.uk (E.A. Gibson), John.Fielden@uea.ac.uk (J. Fielden).

https://doi.org/10.1016/j.dyepig.2022.110244
Received 29 October 2021; Received in revised form 11 February 2022; Accepted 10 March 2022

properties, and p-DSSC performance of three new dyes based on the indolium acceptor group and triarylamine donor with pyridine anchors, supported by TD-DFT calculations. These permit comparison with our prior work on pyridyl anchored pyridinium sensitizers, and carboxylate anchored indoliums. The results seem to confirm that pyridine is a suboptimal anchoring group for dyes with positively charged acceptors, as performances fall well short of those seen for indoliums with carboxylate anchors. Nonetheless, the study also clearly shows that indolium is a more powerful acceptor than pyridinium or the dicyano group, with TD-DFT calculations indicating that the indolium dyes combine strong donor-acceptor communication (and thus high light absorption), with a high degree of charge separation in the excited state. This produces a >100% improvement in device performance *vs* the best pyridinium dye.

## 2. Experimental

**Materials and Synthetic Procedures.** Full details of materials and synthetic methods are provided in the supplementary data.

**General Physical Measurements.** $^1$H NMR and $^{13}$C NMR spectra were recorded on a Bruker Ascend 500 MHz spectrometer. Elemental analyses and mass spectrometry were outsourced to London Metropolitan University, and the UK National Mass Spectrometry Service at Swansea University respectively. Electronic absorption spectra were recorded on an Agilent Cary60 UV–Vis spectrophotometer. Fluorescence spectra were obtained using an Edinburgh Instruments FS5. Electrochemical data were obtained using Autolab PGSTAT30 and PGSTAT302 potentiostat/galvanostats. A single-compartment cell was used with an Ag wire pseudo reference electrode, platinum working electrode and Pt wire auxiliary electrode, the supporting electrolyte was $[N(C_4H_9\text{-}n)_4]BF_4$ [14] in dry acetonitrile. Solutions containing ca. $10^{-3}$ M analyte (0.1 M electrolyte) were degassed by purging with nitrogen. All $E_{1/2}$ values were calculated from $(E_{pa} + E_{pc})/2$ at a scan rate of 100 mV s$^{-1}$, referenced to internal Fc/Fc$^+$, and converted to NHE using Fc/Fc$^+$ = 0.69 V vs NHE.

**Solar Cell Assembly** Glass substrates for the photocathodes (Pilkington TEC 15) and counter electrodes (Pilkington TEC 8) were cut to size (18 × 15 mm) and washed. Substrates were cleaned using an ultrasonic bath using firstly soapy water, secondly 0.1 M HCl in ethanol, and finally ethanol. The glass surfaces were then cleaned using a Novascan PSD Series Digital UV Ozone System in preparation for use.

A sol-gel NiO precursor containing anhydrous $NiCl_2$ (1 g) and a triblock co-polymer, F108 (poly(ethylene glycol)-block-poly(propylene glycol)-block-poly(ethylene glycol) (1 g) dissolved in EtOH (6 ml) and deionised water (3 ml) was prepared and left to age for 14 days. Before use, the solution was centrifuged to remove any remaining solids. To prepare the NiO electrodes, the precursor solution was applied to the substrate via the doctor blade method, using Scotch Magic tape as a spacer (0.25 cm$^2$ active area). Films were sintered in a Nabertherm B150 Chemical Oven in air at 450 °C for 30 min. This process was repeated using two additional layers of precursor solution to increase layer thickness, which was measured using a DEKTAK $^3$ST Profilometer to be 1.2 μm (±0.1 μm) for a 3 layer film. The NiO electrodes were submerged in solutions of dye (0.3 mM) in dry acetonitrile for 48 h at room temperature. Upon removal from the dyebath, the films were rinsed with more acetonitrile and allowed to air dry.

Counter electrode substrates had a small hole (approx. 1 mmØ) drilled in the centre to allow electrolyte to be added in the assembly stage. The substrate was platinized [3,15] by applying $H_2PtCl_4$ (4.8 mM, 10 μL cm$^{-2}$) dropwise onto the conducting surface. The electrodes were then heated for 15 min at 450 °C, and allowed to cool to room temperature.

To assemble devices, the as prepared photocathode and counter electrode were sandwiched face to face using a thermoplastic frame (Surlyn, 60 μm thickness) as a spacer. An electrolyte containing LiI (1 M) and $I_2$ (0.1 M) in dry acetonitrile was introduced into the device through the pre-drilled hole via vacuum backfilling. The cells were sealed with another Surlyn piece and a glass cover slip.

**Device Measurements** Dye loadings were calculated from dye bath measurements (Fig. S13), using the change in absorbance during the soaking process. These gave reasonable agreement (within 30%) with estimates produced by measuring the film absorbances. An Ivium CompactStat potentiostat was used to take current-voltage measurements of devices in both the dark and under AM 1.5 simulated sunlight from a class AAA xenon solar simulator. The device working area was masked with a black aperture (0.16 cm$^2$). The applied voltage was swept from 0.1 V to −0.1 V at a scan rate of 5 mV s$^{-1}$. Incident photon to current conversion efficiency (IPCE) measurements were conducted by passing light from the Xe lamp (Newport, 300 W) through a monochromator (Oriel Cornerstone 130 1/8 m) at 10 nm steps between 400 and 800 nm and measuring the current output of the device vs. a calibrated Si photodiode using an Ivium CompactStat potentiostat.

**DFT calculations** were carried out using the ADF suite of programs [16]. Both geometry optimsation and property calculations were carried out using the B3LYP functional (20% Hartree-Fock exchange) [17] and the ADF double-ζ, single polarisation function DZP basis set. This is comparable to the commonly used 6–31g* basis set, prior work with related pyridinium and dicyano acceptor dyes has indicated that the using larger triple-ζ and augmented basis sets (TZP, AUG-DZP) increases computational expense, without signficantly changing results [12b]. Calculations of the electronic spectra were carried out by TD-DFT using the EXCITATION modules implemented in the ADF program [18] and were based on the optimized geometries, with no frozen core. The EXCITEDGO module was used to calculate geometries of the first excited states of analogues where the hexyl group was replaced by a methyl group - convergence is extremely slow with hexyl, and computed spectra for the methyl analogues are virtually identical to those of **1** to **3**. Ground-to-first excited state dipole moment changes ($\Delta\mu_{12}$) were calculated by subtracting the ground state dipole moment from the excited state dipole moment. Solvent (acetonitrile) was introduced using COSMO with Klamt atomic Radii. The subkey NOCSMRSP was applied to prevent induced electronic charges (which respond on a much slower timescale than electronic excitations) from influencing COSMO surface charges, together with the ALLPOINTS key.

## 3. Results and discussion

### 3.1. Dye synthesis, photophysical and electrochemical properties

Structures of the three new dyes are displayed in Fig. 1, and schemes (S1 to S3) describing the overall synthetic routes are provided in the SI. The strategy taken was identical to that described previously for pyridinium and dicyano acceptors with the same three donor/anchoring groups [12b]. Triarylamine cores derivatised with formyl thiophene groups were synthesized starting from diphenylamine for **1**, through N-arylation followed by bromination and Suzuki coupling; and from 4-bromotriphenylamine for **2** and **3**, by Suzuki coupling, iodination, and a further Suzuki coupling. Then, for all dyes, a Knoevenagel condensation was used to attach the indolium acceptor. Thus, all three dyes can be accessed starting from commercial starting materials in 5 steps (including synthesis of the indolium precursor).

UV–visible absorption spectra of **1** to **3** in acetonitrile are shown in Fig. 2 and the data are summarised in Table 1. The absorption $\lambda_{max}$ values are substantially (up to 100 nm) red shifted compared to those of analogous dicyano or pyridinium acceptor dyes [12b], but show similar trends within the series. All three dyes showed a strong, low energy peak assigned to intramolecular charge transfer (ICT) from the donor triarylamine group to the indolium acceptor. The $\lambda_{max}$ of this peak red-shifts nearly 50 nm upon replacing the pyridyl binding group of **1** with the phenyl pyridyl unit in **2**, as the electron withdrawing effect of the pyridyl ring on the donor N is attenuated. In compound **3**, an intermediate value is seen as the donor N carries two weakly electron withdrawing phenylpyridyl groups. Logically, the extinction coefficient associated

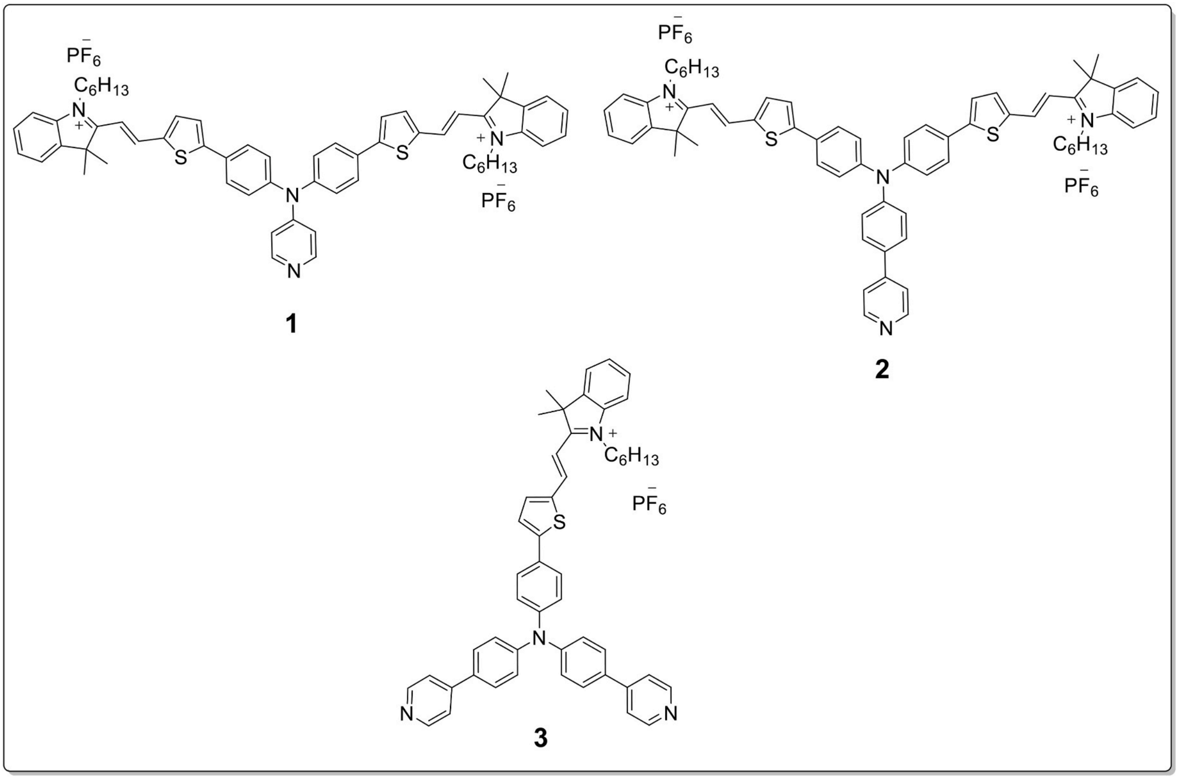

**Fig. 1.** Chemical structures of the dyes **1** to **3** used in this study.

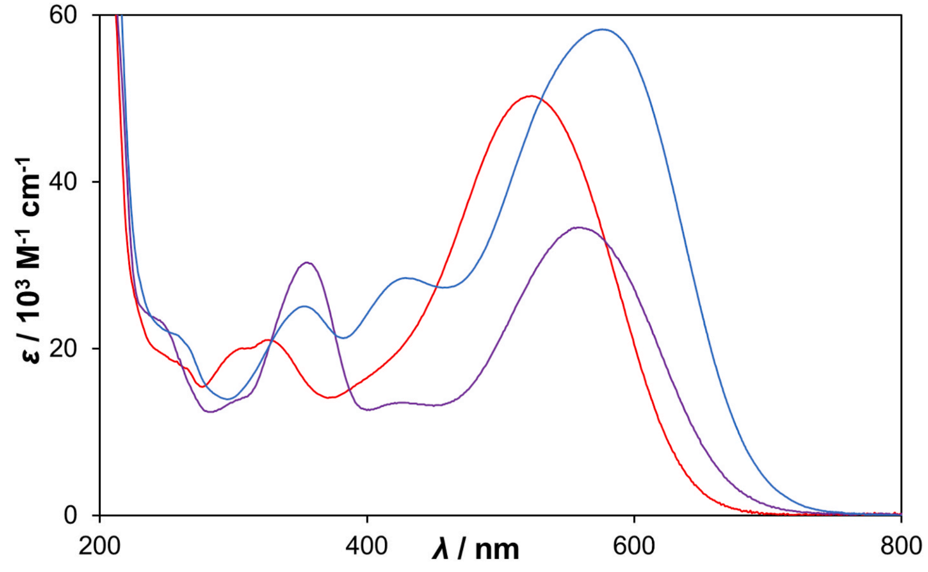

**Fig. 2.** UV–Vis spectra of **1** (red), **2** (blue) and **3** (purple) in MeCN.

with this band is larger in the *bis*-acceptor systems **1** and **2** than in *mono*-acceptor **3**. The three dyes are all weakly emissive (Fig. S1) when excited in the ICT band, with $\lambda_{\mathrm{em}}$ values following the same general trend as $\lambda_{\mathrm{max}}$, although Stokes shifts are larger for **2** (278 nm) and **3** (291 nm) than for **1** (222 nm).

All three dyes show another visible transition at *ca.* 400–410 nm (shoulder in **1**), comparison of **3** with the spectra of its thiophenylaldehyde precursors **P8** and **P9** (Fig. S2) suggests this may arise from processes involving the thiophene group. Compounds **2** and **3** both show a peak at *ca.* 350 nm, absent in **1** and strongest in *bis*-phenylpyridyl **3**, implying it is associated with the phenylpyridine groups. This assignment is also supported by UV–vis spectra (Fig. S2) of the *bis*-bromophenyl, mono-aldehyde (**P8**) and *bis*-phenylpyridyl, mono-aldehyde (**P9**) precursors to **3**, which show a strong peak emerge at 363 nm after connection of the pyridyl groups in **P9** – the slight red shift compared to **2** and **3** is consistent with the phenyl groups and the donor-N being more electron rich in the absence of the indolium acceptor. It is also consistent with TD-DFT calculations (see below and SI) showing transitions between 350 and 380 nm in **2** and **3** that involve both N-phenyl to pyridine charge transfer, and transitions from the phenylpyridine units to the thiophene bridges. Based on energies, the other transitions of all three dyes are considered to be largely π→π* in nature,

**Table 1**

Optical and electrochemical properties of **1** to **3**.

| Dye | $\lambda_{max}{}^{a}$/ nm | $E_{max}$/ eV | $\epsilon/10^3$ M$^{-1}$ cm$^{-1}$ | $\lambda_{em}{}^{a}$/ nm | D$^0$/D$^+$, $E_{pa}$ or $E_{1/2}$ *vs* NHE/V (ΔE/mV) | D$^0$/D$^-$, $E_{pc}$ *vs* NHE/V | $E_{0\text{-}0}{}^{b}$/ eV | Calcd HOMO-LUMO$^c$/eV | Calcd HOMO$^d$ energy/ eV vs vacuum | Calcd LUMO$^d$ energy/ eV vs vacuum |
|---|---|---|---|---|---|---|---|---|---|---|
| 1 | 523 | 2.37 | 49.9 | 745 | *ca.* 1.70$^e$ | −0.22 | 2.02 | 2.04 | −5.989 | −3.701 |
| 2 | 578 | 2.14 | 58.3 | 856 | 1.40 (186) | −0.24 | 1.81 | 1.83 | −5.810 | −3.709 |
| 3 | 561 | 2.21 | 34.3 | 852 | 1.31 (96) | −0.28 | 1.85 | 1.96 | −5.720 | −3.562 |

(a) Absorption and emission spectra recorded in $CH_3CN$ solution. (b) The HOMO-LUMO gap $E_{0\text{-}0}$ calculated from intersection of the normalised absorption and emission spectra (for **2** and **3**). For **1** the midpoint between the absorption and emission peaks (in wavenumber) was used due to contributions from a higher energy process near the intersection. (c) Lowest energy TD-DFT calculated UV–vis transition (HOMO-LUMO), see experimental for details. (d) Extracted from TD-DFT calculation of electronic spectrum. (e) Poorly defined, difficult to distinguish from solvent oxidation. Electrochemical data were obtained using 0.1 M $NBu_4BF_4$ in $CH_3CN$ as electrolyte, with an analyte concentration of *ca.* 1 mM and scan rate 100 mV s$^{-1}$. Potentials referenced to internal Fc/Fc$^+$ and converted to NHE using Fc/Fc$^+$ = 0.69 V vs NHE.

although TD-DFT does indicate some charge transfer character in the higher energy features of **1** and **3** (see below and SI).

Cyclic voltammetry reveals reductions (Table 1, Fig. S2) at around −0.25 V vs NHE for all three compounds, that are irreversible on the timescale of the measurements. These are assigned to the indolium acceptor and are similar, but slightly positively shifted compared to those previously reported for indoliums [10,12a,13]. The potential is significantly less negative than for related pyridinium and dicyano acceptor dyes, showing the increased strength of the indolium acceptor. Irreversible redox potentials cannot be determined with sufficient accuracy to be certain that the trend in the reduction potentials of **1** to **3** (more negative from **1** to **3**, with differences of up to 40 mV) is real, but it is also reflected in the calculated LUMO energies, which get higher in the order **1** < **2** < **3**. This is logical, as the donor becomes more electron rich from **1** to **2** as the phenyl spacer reduces the influence of the pyridine ring, and again from **2** to **3** as the number of indolium acceptor units falls (one in **2**, two in **3**), and shows that the donor weakly influences the reduction of the acceptor. In all three compounds, oxidation of the donor is observed at higher potentials than for related systems with weaker acceptors. The process appears to be quasi-reversible for **3**, significantly less reversible for **2**, and irreversible for **1**, preventing meaningful comparison of the potentials but it is clear that in all cases, the dye oxidation potentials are much more positive than the top of the NiO VB (0.54 V vs NHE) [19], indicating that hole transfer to NiO is energetically favourable. Electron transfer from the dye acceptors to $I_3^-$ ($I_3^-/I_2^{\bullet -}$ = −0.2 V vs NHE [19]) is also energetically favourable but with a weaker driving force, making the computed higher energy LUMO for **3** (reflected in the measured, irreversible electrode potentials) potentially significant in favouring onward electron transfer.

### 3.2. DFT calculations

DFT and TD-DFT calculations were performed on **1** to **3** using the Amsterdam Density Functional (ADF) software package, with the B3LYP functional and DZP basis set [16–18]. Acetonitrile solvent was added using COSMO. The trend in the lowest energy transitions calculated by TD-DFT (all HOMO→LUMO) matches that of both the experimental $E_{max}$ values and $E_{00}$ values, and for **1** and **2** in particular the computed lowest energy transition is a very close quantitative match for $E_{00}$. Computed spectra (Fig.s S6 to S8, SI) also replicate higher energy features reasonably well, although both energies and intensities (compared to lower energy processes) are underestimated in places.

Analysis of the orbital-to-orbital transitions (Tables S1–S3, Figs. S9–S11) reveals that in all cases, the lowest energy (and strongest) transitions involve charge transfer (CT) from a HOMO based predominantly on the triarylamine unit, to a LUMO based largely on the thiophene bridge and indolium. The higher energy transitions tend to involve more π→π* character (and thus a shorter overall CT distance), or CT in the opposite direction. Specifically, for all three dyes, transitions between 2.69 and 3.06 eV (close to the *ca.* 410 nm band or shoulder observed in the experimental spectra) involve transitions from deeper lying HOMO-1/HOMO-2 orbitals to the same LUMO/LUMO+1 orbitals involved in the lower energy CT transitions. However, these HOMO-1/2 orbitals are less concentrated on the triarylamine, and spread more onto the thiophene bridge and acceptor, giving the transitions weaker CT and more π→π* character. Transitions calculated at *ca.* 3.44 and 3.45 eV for **2** and 3.33, 3.45 and 3.46 eV for **3** all show involvement of the phenylpyridine groups (Tables S2 and S3, Figs. S10 and S11). For both compounds, the transitions at around 3.45 eV have little overall CT character as there are contributions from the phenylpyridines providing both donor, and acceptor orbitals. However, the 3.33 eV transition of **3** shows a CT process from the triarylamine-based HOMO, to a phenylpyridine-based LUMO+1 - opposing the desired charge transfer direction – and another CT transition to the LUMO+1 is found for **3** at high energy (4.34 eV). In **1**, calculated transitions at 3.71 and 3.81 eV have broadly similar character to the *ca.* 3.45 eV transitions of **2** and **3**, the higher energy being consistent with the smaller pyridyl (rather than phenylpyridyl π-system) and the 320 nm band observed in the experimental spectrum.

Overall, the computational picture is very similar to our findings for analogous structures with dicyano and pyridinium acceptors [12b]. However, there are some contrasts that are consistent with the higher extinction coefficients measured experimentally for the indolium dyes. In all cases, it appears that there is more spatial overlap between donor and acceptor orbitals for the indolium dyes than there is for pyridinium or dicyano acceptors (Fig. 3) – that is, there is more extension of the LUMO onto the bridge and triarylamine unit, and more extension of the HOMO onto the bridge, than for either of the other two acceptors. Similar results are seen for other indolium dyes [12a], and are consistent with better donor-acceptor communication and thus the higher extinction coefficients obtained for indoliums.

Despite this, the distributions of the excited state HOMOs for the methyl analogues **1Me** to **3Me** (excited state geometry optimisations of **1** to **3** proved too computationally demanding due to the hexyl group, but computed spectra for the methyl analogues are almost identical – see Fig.s S6 to S8) are very similar to those previously calculated for the pyridinium analogues (Fig. 4 and Fig. S12), suggesting that the indoliums are just as effective at separating charge – and better than the dicyano systems. This appears to be confirmed by the calculated ground to first excited state dipole moment change ($\Delta\mu_{12}$) for **3Me**, which is very similar to that of the analogous pyridinium dye **3Pyd** both overall, and along the *z*-axis (defined such that the donor-acceptor axis runs parallel to *z*, Fig. 5). Smaller $\Delta\mu_{12}$ values are obtained for **1** and **2** *vs* pyridinium analogues (Tables S4 and SI), but this is likely a consequence of more complex ground-to-excited state conformational changes in the *bis*-acceptor structures, and the values are still around 50% higher than found for the dicyano systems. Thus, high performance in photoinduced charge separation can be expected from the indolium dyes because they combine a strong acceptor giving broad spectrum absorption (with adequate potential for onward electron transfer, *vide supra*), with strong donor acceptor communication and a high degree of charge separation between ground and excited state. This is an unusual combination, as often increased donor-acceptor communication comes at the cost of charge separation.

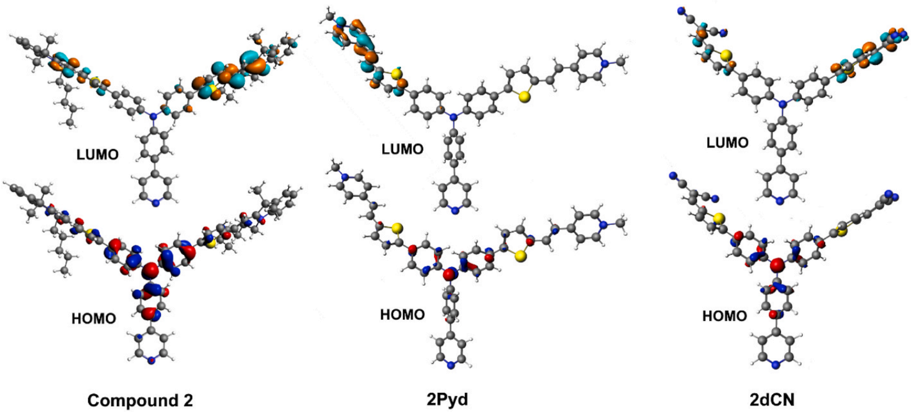

**Fig. 3.** HOMO and LUMO orbitals of compound **2** and pyridinium (**2Pyd**) and dicyano analogues (**2dCN**), showing increased spatial overlap of the donor and acceptor orbitals in the indolium dye **2**. Data for **2Pyd** and **2dCN** is taken from reference 12b.

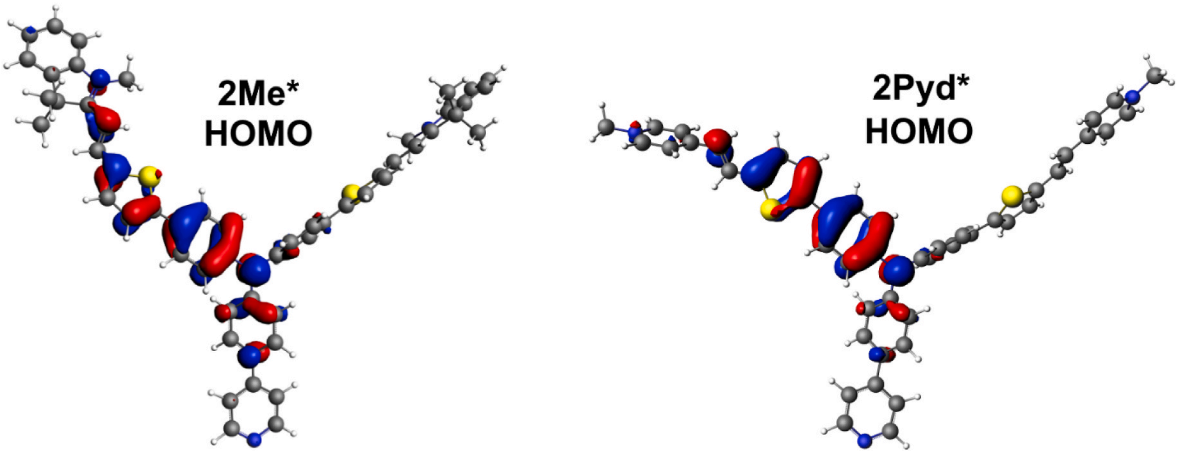

**Fig. 4.** Excited state HOMOs of methyl analogue of **2** (**2Me**) and pyridinium analogue **2Pyd**.

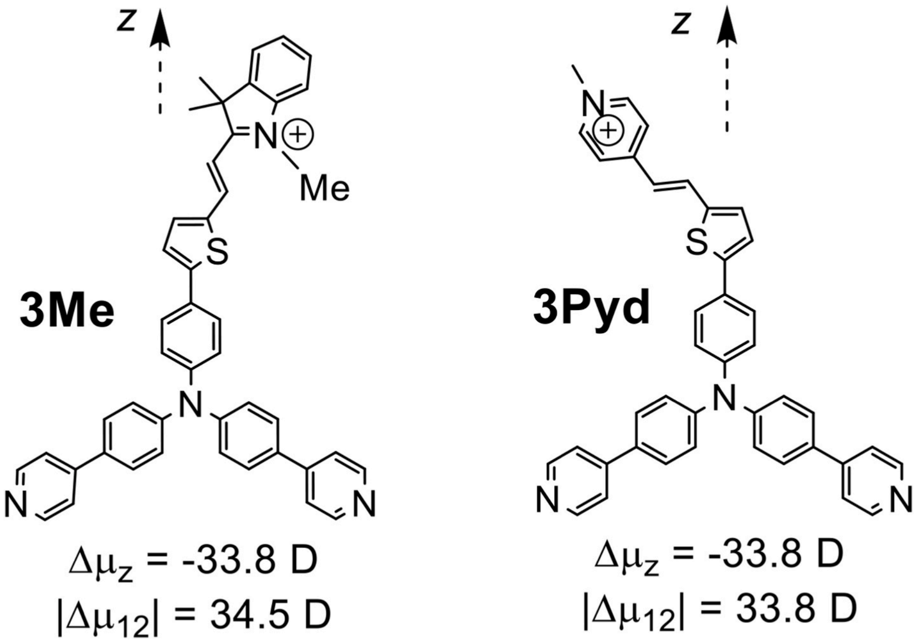

**Fig. 5.** Structures and ground-to-first excited dipole moment changes of indolium **3Me** and pyridinium analogue **3Pyd**.

### *3.3. Solar Cell Assembly and photovoltaic performance*

Fig. 6 shows the absorption spectra of **1** to **3** on 3-layer NiO films after immersion for 48 h. The intermolecular charge transfer peaks broaden (for all dyes) and blue shift (for **1** and **2**) slightly compared to the solution spectra, but the transitions are still defined. Dye loadings for **1** to **3** and the benchmark **P1** [20] (Table 2), calculated from the change in absorbance of the soaking solutions (Fig. S13), showed that all of the cationic dyes **1** to **3** load less well than **P1** (which is negatively charged once deprotonated), consistent with repulsion from the positively charged NiO surface. However, there is no clear dependence on charge within the series **1** to **3**. These results, as well as being consistent with previous findings that dye loading is a limitation to the performance of p-DSSCs based on cationic dyes, suggest that a complex range of factors must influence dye loading, including the space required by the dye at the surface and the basicity of the pyridine as well as charge.

The photovoltaic performance (AM1.5) of champion p-DSSCs based on NiO sensitized with **1** to **3** and **P1**, using an $I^-/I_3^-$ redox mediator, is also summarised in Table 2 (for *J-V* curves see Fig. S14 and for average devices Table S5). It can be seen that all of the cells based on the pyridine anchored indolium dyes investigated here have high $V_{OC}$ and improved fill factor relative to the **P1** reference cell. This enables the best performing indolium-based cell (compound **2**) reach a higher power conversion efficiency (PCE, $\eta = 0.097\%$) than the **P1** cell despite lower $J_{sc}$. Improved $V_{OC}$ compared to **P1** has previously been found for pyridine anchored dicyano dyes, and the binding mechanism of the pyridine to NiO suggested as an explanation [11]. However, a very wide range of factors can influence $V_{OC}$ and FF, so it is not possible to confidently link this result to any specific structural feature of **1** to **3**.

That phenylpyridyl *bis*-indolium **2** shows the best overall performance is consistent with prior findings for dicyano and pyridinium analogues [12b] – but $\eta$ for **2** is more than 1.5 × better than the analogous dicyano and nearly 3 × better than the analogous pyridinium, thanks to higher $J_{sc}$. This is a consequence of the better light absorption properties of the indoliums, whose $\lambda_{max}$ values are around 100 nm to the red of the pyridiniums, and also improved dye loadings obtained in this study. Indeed, IPCE spectra (Fig. 7) show that **2** and **3** both harvest photons beyond 700 nm – while their pyridinium analogues produce no appreciable photocurrent when $\lambda > 650$ nm [12b]. Cells based on reference **P1** have also been shown to produce minimal photocurrent beyond 650 nm, but their peak IPCE is higher – around 18% between 450 and 550 nm in cells with similar performance to ours [20a], and up to 63% in the best devices [20b] – consistent with the higher $J_{SC}$ observed here. The longer alkyl chains used to quaternise the indoliums may also confer an advantage in preventing recombination: lower dark currents (Fig. S14) for **1** and **2** (two hexyl groups) *vs* **3** (one hexyl group) are consistent with the alkyl groups lowering recombination, as shown previously through measurement of charge lifetimes [12a].

**Table 2**
Film absorption, loading and Photovoltaic parameters under the AM1.5 simulated solar spectrum including open circuit voltage ($V_{OC}$), short circuit current ($J_{SC}$), fill factor (*FF*) and efficiency ($\eta$) of champion NiO p-DSSCs based on **1** to **3**.

| Dye | Film $\lambda_{max}$/ nm | Dye Loading/nmol cm$^{-2}$ | $V_{OC}$/ mV | $J_{SC}$/mA cm$^{-2}$ | *FF*/ % | $\eta$/% |
|---|---|---|---|---|---|---|
| 1 | 501 | 25 | 89 | 1.65 | 34 | 0.044 |
| 2 | 565 | 17 | 97 | 3.04 | 33 | 0.097 |
| 3 | 562 | 26 | 99 | 2.26 | 34 | 0.077 |
| P1 | 498 | 34 | 71 | 3.82 | 27 | 0.079 |

Within the indolium series, it can be seen that while the trend *vs* the phenyl spacer free, *bis*-indolium **1** is similar to that seen for pyridinium dyes (*ca.* 100% increase in PCE for **2** *vs* **1**), the *bis*-phenylpyridyl architecture (**3**) found to perform poorly with pyridinium and dicyano acceptors [12b] gives a much more competitive result with the indolium acceptor. In fact, the PCE of this architecture with indolium is 5.5 × higher than with pyridinium. The reason for this is not entirely clear. Increased $J_{sc}$ will result from improved harvesting of low energy photons by **3** compared to its pyridinium analogue (**3Pyd**), but this is the case for all of the indoliums, moreover TD-DFT calculations on **3** and **3Pyd** do not show any major differences in charge distribution which could affect electron transfer to the mediator. The only molecular explanation would thus appear to be the higher energy LUMO of **3** compared to the other

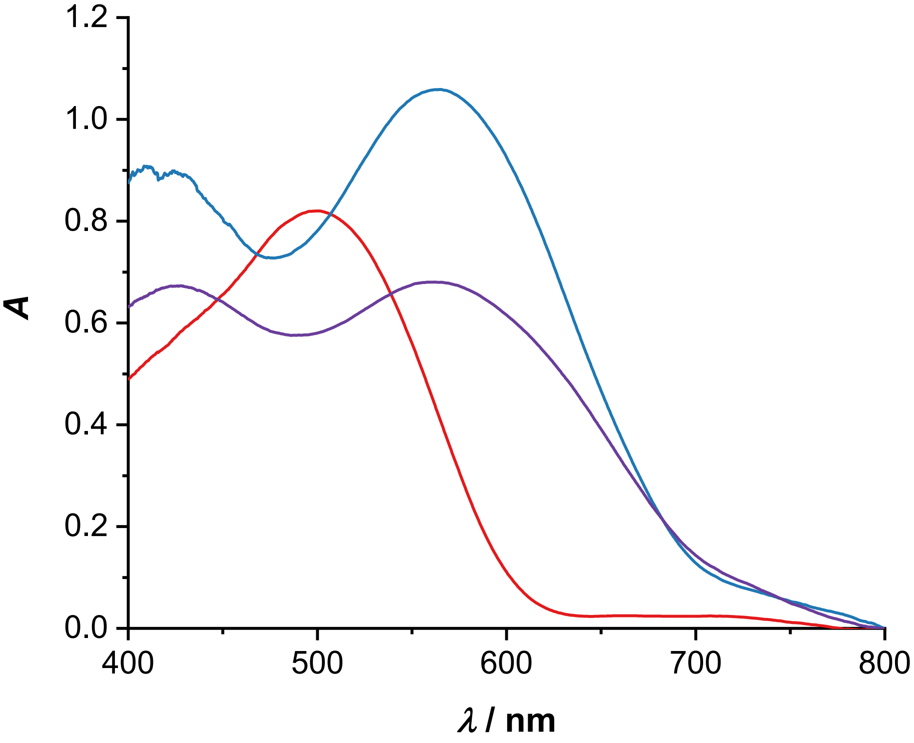

**Fig. 6.** UV–visible absorption spectra of **1** (red), **2** (blue) and **3** (purple) on 3-layer NiO films with NiO subtracted.

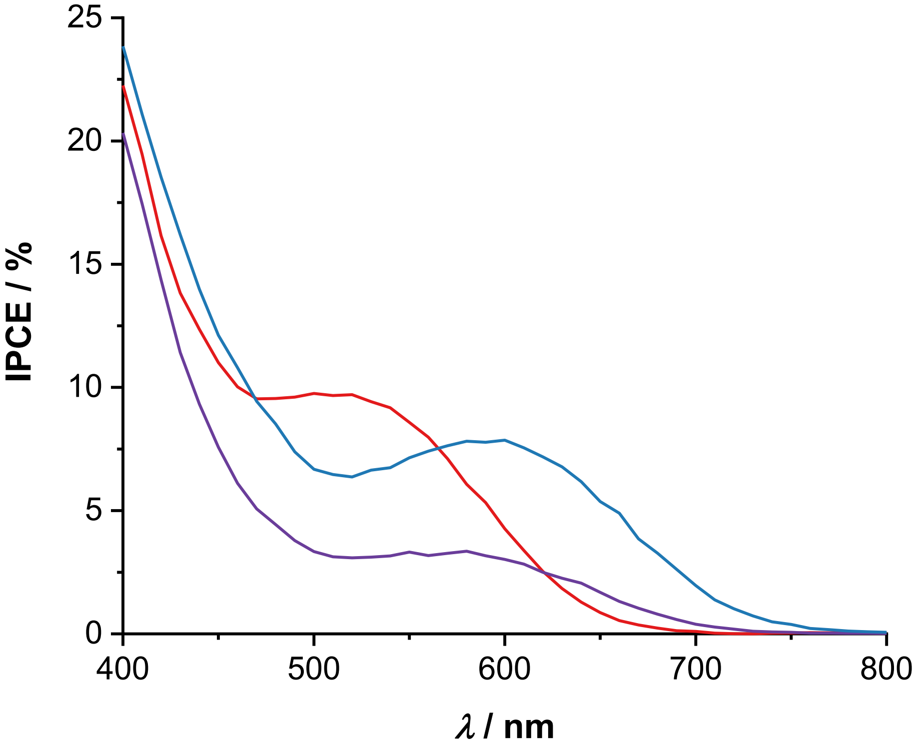

**Fig. 7.** IPCE for NiO p-DSSCs sensitized with compounds **1** (red), **2** (blue) and **3** (purple).

indolium dyes – *ca.* 0.15 eV above that of both **2** and **3**, and reflected in the more negative irreversible D/D$^-$ redox potential for **3**. This would give an increased driving force for electron transfer to $I_3^-$ from **3** compared to **1** and **2**, which is significant because the driving force for electron transfer from D$^-$ to $I_3^-$ is relatively small for all of the indoliums. Thus, in the indolium series an increased driving force for electron transfer to the mediator potentially compensates the weaker light absorption and less optimal electronic structure of the *mono*-acceptor system.

## 4. Conclusions

Three new dyes based on triarylamine cores, with indolium acceptors and pyridine anchors have been successfully synthesized, characterized and applied in p-type DSSCs. These have high extinction coefficients and light absorption profiles extending to 700 nm and beyond, with TD-DFT calculations indicating an ideal combination of strong donor-acceptor communication, and a high degree of charge separation in the excited state. Similar to prior work with dicyano and pyridinium acceptors, the best p-DSSC performance ($\eta = 0.097\%$) was obtained in an architecture combining two indolium acceptor groups with a phenyl pyridine anchor, representing a near three-fold improvement on the pyridiniums as a result of the improved long-wavelength light absorption. As with other cationic dyes, however, dye loading is lower than for neutral or anionic references, potentially limiting device output.

## CRediT authorship contribution statement

**Anil Reddy Marri:** Investigation, Synthetic Chemistry, Electrochemistry, UV–vis spectroscopy, Writing – original draft, Funding acquisition. **Heather Flint:** Investigation, Solar Cell Assembly and Performance, Writing – original draft. **Elizabeth A. Gibson:** Funding acquisition, Supervision, Conceptualization, Investigation, solar cells, Writing – review & editing. **John Fielden:** Funding acquisition, Supervision, Conceptualization, Investigation, computation, Writing – review & editing.

## Declaration of competing interest

The authors declare that they have no known competing financial interests or personal relationships that could have appeared to influence the work reported in this paper.

## Acknowledgements

We thank the UK EPSRC National Mass Spectrometry Facility for MS. ARM thanks the EU for Marie Skłodowska Curie Fellowship No. 656658 “NanoCuI”, and JF the Royal Society for Research Grant RG140578. EAG thanks the EU for ERC starting grant p-TYPE 715354.

## Appendix A. Supplementary data

Supplementary data to this article can be found online at https://doi.org/10.1016/j.dyepig.2022.110244.

## References

[1] (a) O'Regan B, Grätzel M. A low-cost, high-efficiency solar cell based on dye-sensitized colloidal TiO2 films. Nature 1991;353:737–40.(b) Hagfeldt A, Boschloo G, Sun L, Kloo L, Pettersson H. Dye-sensitized solar cells. Chem Rev 2010;110:6595–663.(c) Clifford JN, Martinez-Ferrero E, Viterisi A, Palomares E. Sensitizer molecular structure-device efficiency relationship in dye sensitized solar cells. Chem Soc Rev 2011;40:1635–46.

[2] (a) Lee C-P, Lin RY-Y, Lin L-Y, Li C-T, Chu T-C, Sun S-S, Lin JT, Ho K-C. Recent progress in organic sensitizers for dye-sensitized solar cells. RSC Adv 2015;5:23810–25.(b) Kakiage K, Aoyama Y, Yano T, Oya K, Fujisawab J, Hanaya M. Highly-efficient dye-sensitized solar cells with collaborative sensitization by silyl-anchor and carboxyl anchor dyes. Chem Commun 2015;51:15894–7.

[3] He J, Lindström H, Hagfeldt A, Lindquist S-E. Dye-sensitied nanostructured p-type nickel oxide film as a photocathode for a solar cell. J Phys Chem B 1999;103:8940–3.

[4] Perera IR, Daeneke T, Makuta S, Yu Z, Tachibana Y, Mishra A, et al. Application of the tris(acetylacetonato)iron(III)/(II) redox couple in p-type dye-sensitized solar cells. Angew Chem Int Ed 2015;54:3758–62.

[5] Powar S, Daeneke T, Ma MT, Fu D, Duffy NW, Götz G, Weidelener M, Mishra A, Bäuerle P, Spiccia L, Bach U. Highly efficient P-type dye-sensitized solar cells based

on tris(1,2-diaminoethane)Cobalt(II)/(III) electrolytes. Angew Chem Int Ed 2013;52:602–5.

[6] (a) Favereau L, Warnan J, Pellegrin Y, Blart E, Boujtita M, Jacquemin D, Odobel F. Diketopyrrolopyrrole derivatives for efficient NiO-based dye-sensitized solar cells. Chem Commun 2013;49:8018–20.(b) Farré Y, Raissi M, Fihey A, Pellegrin Y, Blart E, Jacquemin D, et al. A blue diketopyrrolopyrrole sensitizer with high efficiency in nickel-oxide-based dye-sensitized solar cells. ChemSusChem 2017;10:2618–25.

[7] (a) Hagfeldt A, Boschloo G, Sun L, Kloo L, Pettersson H. Dye sensitized solar cells. Chem Rev 2010;110:6595–663.(b) Odobel F, Le Pleux L, Pellegrin Y, Blart E. New photovoltaic devices based on the sensitization of p-type semiconductors: challenges and opportunities. Acc Chem Res 2010;43:1063–71.(c) Odobel F, Pellegrin Y, Gibson EA, Hagfeldt A, Smeigh AL, Hammarström L. Recent advances and future directions to optimize the performances of p-type dye-sensitized solar cells. Coord Chem Rev 2012;256:2414–23.(d) Odobel F, Pellegrin Y. Recent advances in the sensitization of wide-band gap nanostructured p-type semiconductors. Photovoltaic and photocatalytic applications. J Phys Chem Lett 2013;4:2551–64.

[8] (a) Yu M, Natu G, Ji Z, Wu Y. p-Type dye sensitized solar cells based on delafossite $CuGaO_2$ nanoplates with saturation photovoltages exceeding 460 mV. J Phys Chem Lett 2012;3:1074–8.(b) Langmar O, Fazio E, Schol P, de la Torre G, Costa RD, Torres T, Guldi DM. Controlling interfacial charge transfer and fill factors in CuO-based tandem dye-sensitized solar cells. Angew Chem Int Ed 2019;58:4056–60.(c) Langmar O, Ganivet CR, de la Torre G, Torres T, Costa RD, Guldi DM. Optimizing CuO p-type dye-sensitized solar cells by using a comprehensive electrochemical impedance spectroscopic study. Nanoscale 2016;8:17963–75.(d) Muñoz-García AB, Benesperi I, Boschloo G, Concepcion JJ, Delcamp JH, Gibson EA, Meyer GJ, Pavone M, Pettersson H, Hagfeldt A, Freitag M. Dye-sensitized solar cells strike back. Chem Soc Rev 2021;50:12450–550.

[9] (a) Ji Z, Natu G, Huang Z, Wu Y. Linker effect in organic donor−acceptor dyes for p-type NiO dye sensitized solar cells. Energy Environ Sci 2011;4:2818–21.(b) Qin P, Linder M, Brinck T, Boschloo G, Hagfeldt A, Sun L. High incident photon-to-current conversion efficiency of p-type dye-sensitized solar cells based on NiO and organic chromophores. Adv Mater 2009;21:2993–6.(c) Chang C-H, Chen Y-C, Hsu C-Y, Chou H-H, Lin JT. Squaraine-arylamine sensitizers for highly efficient p-type dye-sensitized solar cells. Org Lett 2012;14:4726–9.

[10] Wood CJ, Summers GH, Gibson EA. Increased photocurrent in a tandem dye sensitized solar cell by modifications in push-pull dye-design. Chem Commun 2015;51:3915–8.

[11] Cui J, Lu J, Xu X, Cao K, Wang Z, Alemu G, Yuang H, Shen Y, Xu J, Cheng Y, Wang M. Organic sensitizers with pyridine ring anchoring group for p-type dye-sensitized solar cells. J Phys Chem C 2014;118:16433–40.

[12] (a) Wood CJ, Cheng M, Clark CA, Horvath R, Clark IP, Hamilton ML, Towrie M, George MW, Sun L, Yang X, Gibson EA. Red-absorbing cationic acceptor dyes for photocathodes in tandem solar cells. J Phys Chem C 2014;118:16536–46.(b) Marri AR, Black FA, Mallows J, Gibson EA, Fielden J. Pyridinium p-DSSC dyes: an old acceptor learns new tricks. Dyes Pigments 2019;165:508–17.

[13] Wood CJ, Summers GH, Gibson EA. Increased photocurrent in a tandem dye-sensitized solar cell by modifications in push-pull dye design. Chem Commun 2015;51:3915–8.

[14] Ibrahim SK. PhD Thesis. University of Sussex; 1992.

[15] For information on the chemistry of $I^-$ oxidation at the Pt counter electrode, see Wood CJ, McGregor CA, Gibson EA. Does iodine or thiocyanate play a role in p-type dye-sensitized solar cells?. Chemelectrochem 2016;3:1827–36.

[16] (a) Te Velde G, Bickelhaupt FM, Baerends EJ, Fonseca Guerra C, van Gisbergen SJA, Snijders JG, Ziegler T. Chemistry with ADF. J Comput Chem 2001;22:931–67.(b) Fonseca Guerra C, Snijders JF, Te Velde G, Baerends E. Towards an order-N DFT method. J Theor Chem Acc 1998;99:391–403.(c) ADF2018.3. SCM, theoretical Chemistry. Amsterdam, The Netherlands: Vrije Universiteit; 2018. http://www.scm.com.

[17] Stephens PJ, Devlin FJ, Chabalowski CF, Frisch MJ. Ab initio calculation of vibrational absorption and circular dichroism spectra using density functional force fields. J Phys Chem 1994;98:11623–7.

[18] van Gisbergen SJA, Snijders JG, Baerends EJ. Implementation of time-dependent density functional response equations. Comput Phys Commun 1999;118:119–38.

[19] Gibson EA, Le Pleux L, Fortage J, Pellegrin Y, Blart E, Odobel F, Hagfeldt A, Boschloo G. Role of the triiodide/iodide redox couple in dye regeneration in p-type dye-sensitized solar cells. Langmuir 2012;28:6485–93.

[20] (a) Qin P, Zhu H, Edvinsson T, Boschloo G, Hagfeldt A, Sun L. Design of an organic chromophore for p-type dye-sensitized solar cells. J Am Chem Soc 2008;130:8570–1.(b) Qin P, Wiberg J, Gibson EA, Linder M, Li L, Brinck T, Hagfeldt A, Albinsson B, Sun L. Synthesis and mechanistic studies of organic chromophores with different energy levels for p-type dye-sensitized solar cells. J Phys Chem C 2010;114:4738–48.